Springer

KSME

Journal of Mechanical Science and Technology 28 (8) (2014) 3285~3299
www.springerlink.com/content/1738-494x
DOI 10.1007/s12206-014-0740-z

Variable structure controller design for steer-by-wire system of a passenger car †

Iman Mousavinejad[1,*] and Reza Kazemi[2]

[1]*School of Mechatronics Engineering, Sharif University of Technology, Tehran, Iran*
[2]*School of Mechanical Engineering, K.N Toosi University of Technology, Tehran, Iran*

(Manuscript Received October 31, 2012; Revised March 22, 2014; Accepted April 18, 2014)

Abstract

The electric power steering (EPS) system was developed and the steer-by-wire (SBW) system achieves the purposes of EPS. The advantages of SBW are packaging flexibility, advanced vehicle control system, and superior performance. No mechanical linkage exists between the steering gear and steering column in the SBW system. The steering wheel and front-wheel steering can be controlled independently. The SBW system consists of two motors controlled by an electronic control unit (ECU). One motor is in the steering wheel and develops the steering feel of the driver and the other motor is in the steering linkage and improves vehicle maneuverability and stability. Moreover, the active front steering (AFS) system can be added to the SBW system. AFS reduces the difference between actual and estimated vehicle yaw rate. Up-to-date information from the steering wheel enables drivers to identify road conditions through the tire force, which should be fed back to the steering wheel. Furthermore, several control algorithms related to the vehicle and motor can be used together through the self-aligning torque, which is fed back to the steering wheel. This study proposes a method to control the vehicle yaw rate through an SBW system. This control method is based on a PID control method for the steering-wheel-motor controller, as well as on a sliding mode control (SMC) method for the front-wheel-motor controller and yaw stability controller. The SBW system is modeled using a bond graph method. Results imply that the controllers are robust enough when in contact with nonlinear properties of tire and road conditions. This study is expected to guide further research on the SBW system.

Keywords: Active front steering; Bond graph; Electronic control unit; Electronic power steering; Sliding mode control

1. Introduction

The steer-by-wire (SBW) system is part of the drive-by-wire (DBW) system that has been increasingly investigated in automobile industries.

Mechanical and hydraulic systems for steering, braking, suspension and throttle functions are replaced with electronic actuators, controllers and sensors by the new DBW system. The conventional linkage between the steering wheel and front wheel is removed in the SBW system and it is operated by electronic actuators. The SBW system is beneficial because it can easily eliminate the interference between driver and the steering system. Other system benefits include

- increase in packaging flexibility,
- simplification of assembly, and
- vehicle mass reduction.

Reducing necessary parts in the SBW system reduces vehicle weight, which leads to effective energy reduction. This particular advantage is improved without mechanical linkage. The danger of a driver being crushed during a front-end collision is removed because of the absence of the steering column. Moreover, using the active front system (AFS) system improves vehicle stability, dynamics, and maneuverability.

The main disadvantage of the SBW system is the absence of direct mechanical feedback to the operator about steering conditions, which must be emulated by an active control system [1].

Nishizaki and Hayama (2000) proposed the SBW system, which uses direct yaw-moment control based on vehicle stability [2]. Setlur et al. (2002) worked on a continuous time-varying tracking controller design for the SBW system in an automated vehicle. This design resulted in a nonlinear tracking controller that forced a vehicle to follow a given reference path or trajectory [3].

Jang et al. (2003) proposed a control method for the SBW system, which uses a bond graph method to model the front wheel motor [1]. Park et al. (2005) recommended using a PI controller as an electronic control unit (ECU) for the rack-actuating SBW system. They also discussed how to develop the ECU using the HILS system [4].

Bajcinca and Cortesao (2005) designed a robust controller for the SBW system based on H∞ techniques [5]. Sung et al. (2007) designed a bilateral controller based on the disturbance

*Corresponding author. Tel.: +98 912 3007331, Fax.: +98 21 22821850
E-mail address: iman.mousavinejad@gmail.com
† Recommended by Associate Editor Cong Wang

observer for the SBW system. The proposed control method enables the driver to feel the virtual impedance through the suppressed slave dynamics [6].

The objectives of this study are as follows:

- The AFS controller is designed based on the SMC method to improve vehicle handling by tracking the reference yaw rate.
- The steering-wheel-motor controller is designed based on the PID control method to improve the steering feel of the driver.
- The front-wheel-motor controller is designed based on the SMC method to improve vehicle stability and maneuverability.

2. Vehicle and tire model

In this study, a two-degree-of-freedom (2-DOF) model is used for the AFS controller design and an eight-degree-of-freedom (8-DOF) model is used as a vehicle controlled plant for control system evaluations through computer simulations.

2.1 8-DOF vehicle model

The 8-DOF model includes three vehicular planar motions plus body roll motion relative to the chassis about the roll axis and the rotational dynamics of four wheels. Fig. 1 illustrates the vehicle model with a coordinate system, degrees of freedom, and external forces. The motion equations for the model are given as follows:

Longitudinal motion

$$m\left(\dot{V}_x - \gamma V_y\right) + m_s h_s \gamma\dot{\phi} = \sum F_x \,. \tag{1}$$

Lateral motion

$$m\left(\dot{V}_y + \gamma V_x\right) - m_s h_s \ddot{\phi} = \sum F_y \,. \tag{2}$$

Yaw motion

$$\mathrm{I}_{zz}\dot{\gamma} - I_{xz}\ddot{\phi} = \sum M_z \,. \tag{3}$$

Roll motion

$$I_{xx}\ddot{\phi} + m_s h_s\left(\dot{V}_y + V_x\gamma\right) - I_{xz}\dot{\gamma} = \sum M_x \,. \tag{4}$$

$\sum F_x$, $\sum F_y$, $\sum M_z$, and $\sum M_x$ are the sums of external forces and moments acting on the vehicle as follows:

$$\sum F_x = F_{x1} + F_{x2} + F_{x3} + F_{x4} \tag{5}$$

$$\sum F_y = F_{y1} + F_{y2} + F_{y3} + F_{y4} \tag{6}$$

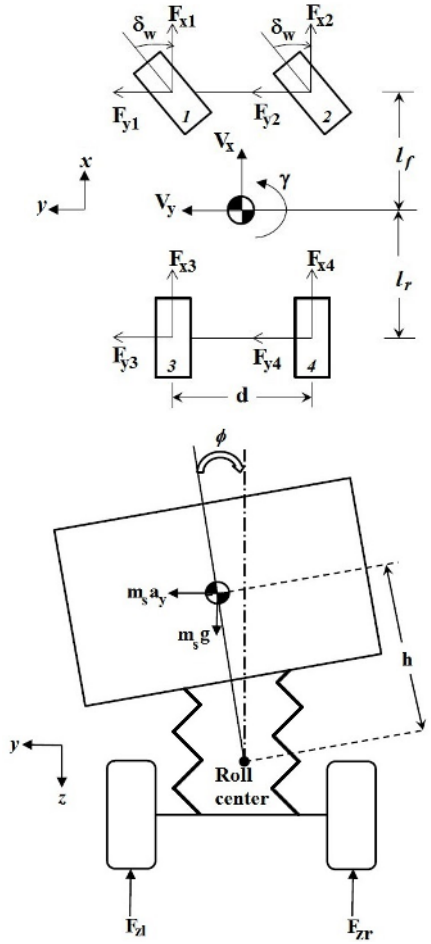

Fig. 1. 8-DOF vehicle model.

$$\sum M_z = l_f\left(F_{y1} + F_{y2}\right) - l_r\left(F_{y3} + F_{y4}\right) + M_{zc} \tag{7}$$

$$\sum M_x = m_s g h_s + M_{\varphi f} + M_{\varphi r} \tag{8}$$

$$M_{zc} = \frac{d}{2}\left[\left(F_{x1} + F_{x3}\right) - \left(F_{x2} + F_{x4}\right)\right] \tag{9}$$

$$M_{\varphi f} = -\left(k_{\varphi f}\varphi + c_{\varphi f}\dot{\varphi}\right) \tag{10}$$

$$M_{\varphi r} = -\left(k_{\varphi r}\varphi + c_{\varphi r}\dot{\varphi}\right). \tag{11}$$

All vehicle parameters are defined in Table 5. $\sum F_x$ is the sum of longitudinal forces in the body-fixed coordinate system of the vehicle from all four tires, and $\sum F_y$ is the sum of lateral forces. F_{xi} and F_{yi} are the resulting longitudinal and lateral forces acting on the ith wheel in the vehicle fixed coordinate system. These forces are related to F_{xwi} and F_{ywi}, which are tire forces along the wheel axes (Fig. 2).

$$\begin{bmatrix} F_{xi} \\ F_{yi} \end{bmatrix} = \begin{bmatrix} \cos\delta_{wi} & -\sin\delta_{wi} \\ \sin\delta_{wi} & \cos\delta_{wi} \end{bmatrix} \begin{bmatrix} F_{xwi} \\ F_{ywi} \end{bmatrix} \quad i = 1,2,3,4 \,. \tag{12}$$

The suspension system is not considered in this modeling.

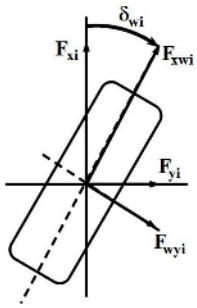

Fig. 2. Wheel coordinate system.

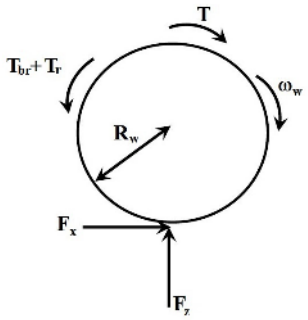

Fig. 3. Free diagram of wheel.

Normal tire forces affect the longitudinal and lateral forces and the self-aligning torque. Consequently, normal tire forces should be modeled as the following equations. Based on quasi-static longitudinal and lateral load transfers, the instantaneous vertical tire load acting on each wheel (F_{zi}) during dynamic maneuvers is the sum of static tire load and the transfer caused by longitudinal acceleration, lateral acceleration, and body roll motion, respectively. This effect is described as follows:

$$F_{z1} = \frac{mgl_r}{2l} - ma_x\frac{h}{2l} - \frac{ma_y l_r h}{ld} + \frac{-\left(k_{\varphi f}\phi + c_{\varphi f}\dot{\phi}\right)}{d} \tag{13}$$

$$F_{z2} = \frac{mgl_r}{2l} - ma_x\frac{h}{2l} + \frac{ma_y l_r h}{ld} + \frac{-\left(k_{\varphi f}\phi + c_{\varphi f}\dot{\phi}\right)}{d} \tag{14}$$

$$F_{z3} = \frac{mgl_f}{2l} + ma_x\frac{h}{2l} - \frac{ma_y l_f h}{ld} + \frac{-\left(k_{\varphi r}\phi + c_{\varphi r}\dot{\phi}\right)}{d} \tag{15}$$

$$F_{z4} = \frac{mgl_f}{2l} + ma_x\frac{h}{2l} + \frac{ma_y l_f h}{ld} + \frac{-\left(k_{\varphi r}\phi + c_{\varphi r}\dot{\phi}\right)}{d} \tag{16}$$

where $l = l_f + l_r$ is the wheel base.

2.2 Wheel equation of motion

The wheel is one of the most significant subsystems for studying vehicular dynamics, particularly in braking and tracking. In accordance with the free diagram of the wheel at the braking and tracking states, the wheel rotational equation of motion is as follows:

$$I_w\dot{\omega}_{wi} = -R_w F_{xi} + T - T_{bri} - T_{ri} \quad i = 1,2,3,4 \tag{17}$$

where T is the driving torque, T_{br} is the braking torque, T_r is the rolling resistance torque, R_w is the dynamic radius of the wheel, I_w is the wheel rotational moment of inertia, and ω_w is the wheel angular velocity. T is equal to zero at braking state and T_{br} is equal to zero at tracking state. Fig. 3 shows that the direction of Fx at tracking state is opposite to the direction of Fx at braking state. The rolling resistance torque is calculated as

$$T_{ri} = f_r F_{zi} R_{wi} \quad i = 1,2,3,4 \tag{18}$$

where f_r is the rolling resistance coefficient, which is typically between 0.01 and 0.02. We assume that $f_r = 0.015$ in this study.

2.3 Tire model

The magic formula is a recently developed empirical method for characterizing tire behavior. This method is used for vehicle handling simulations. In its basic form, the method fits experimental tire data to characterize the relationships between the cornering force and slip angle, the self-aligning torque and slip angle, or the braking effort and skid. The PAC 2002 (Pacejka, 2002) is the latest version of the well-known magic formula and is used to model the vehicle. The general form of the formula is as follows:

$$\begin{aligned} y(x) &= D\sin\left\{C\tan^{-1}\left[Bx - E\left(Bx - \tan^{-1}(Bx)\right)\right]\right\} \\ Y(X) &= y(x) + S_v \\ x &= X + S_h \end{aligned} \tag{19}$$

where $Y(X)$ represents the cornering force, self-aligning torque, or braking effort and X denotes the slip angle or skid. Coefficient B is the stiffness factor, C is the shape factor, D is the peak factor, and E is the curvature factor. S_h and S_v are the horizontal shift and vertical shift, respectively. For further information, refer to Refs. [7, 8].

2.4 2-DOF bicycle model

The 2-DOF model is a good representation of lateral vehicular dynamics in the linear handling region. The model is used to design the AFS controller. The states in this model are lateral motion and yaw motion. This model is described by the following state equations with small wheel angle and constant forward speed assumptions:

$$m\left(\dot{V}_y + \gamma V_x\right) = F_{yf} + F_{yr} \tag{20}$$

$$I_{zz}\dot{\gamma} = l_f F_{yf} - l_r F_{yr}\ . \tag{21}$$

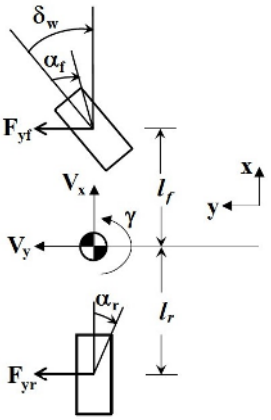

Fig. 4. 2-DOF vehicle model.

The longitudinal velocity V_x is assumed to be strictly constant for basic motion and essentially constant for perturbed motion; thus, V_x is a parameter rather than a variable. The front wheel angle δ_w is also assumed to be a small angle with longitudinal forces at zero.

Assuming a small angle, we can readily express the slip angles as the ratio between lateral velocity (with regard to wheel pointing direction) and rolling velocity as follows:

$$\alpha_f = \frac{V_y + l_f\gamma}{V_x} - \delta_w, \quad \alpha_r = \frac{V_y - l_r\gamma}{V_x}. \tag{22}$$

The lateral forces are assumed to have a linear function with the slip angles as follows:

$$\begin{aligned} F_{yf} &= -C_f\alpha_f \\ F_{yr} &= -C_r\alpha_r \end{aligned} \tag{23}$$

where C_f and C_r are the positive cornering stiffness of both tires for the entire axle, which is twice the cornering stiffness of a single tire.

Combining Eqs. (20)-(23), we obtain the following state equation:

$$\begin{aligned} \dot{X} &= AX + Bu \\ X &= \begin{Bmatrix} V_y \\ \gamma \end{Bmatrix}, u = \{\delta_w\} \\ A &= \begin{bmatrix} -\frac{\left(C_f + C_r\right)}{mV_x} & -\frac{\left(l_fC_f - l_rC_r\right)}{mV_x} - V_x \\ -\frac{\left(l_fC_f - l_rC_r\right)}{I_{zz}V_x} & -\frac{\left(l_f^2C_f + l_r^2C_r\right)}{I_{zz}V_x} \end{bmatrix} \\ B &= \begin{bmatrix} \frac{C_f}{m} \\ \frac{l_fC_f}{I_{zz}} \end{bmatrix}. \end{aligned} \tag{24}$$

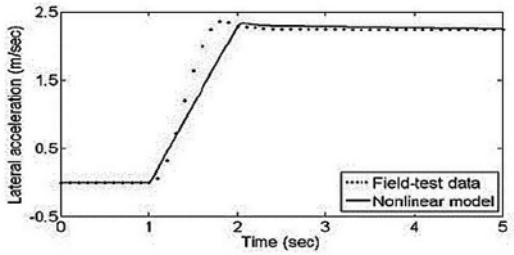

Fig. 5. Vehicle lateral acceleration.

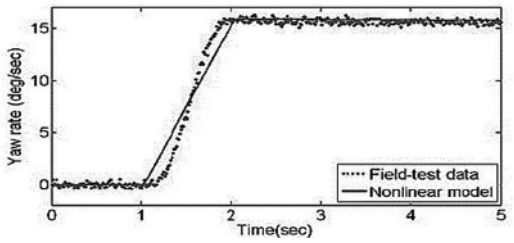

Fig. 6. Vehicle yaw rate.

3. 8-DOF model validation

Model system validation is one of the most important steps in the simulation process. Therefore, the designer must verify the dynamic model using tested-actual vehicle[1] results for the same maneuver.

The vehicle parameters of a compact car were used for the vehicle model. A constant-speed-variable steer test defined in SAE J266 [9] was performed on the model. Figs. 5 and 6 show a comparison of the vehicle lateral acceleration and yaw rate response between the 8-DOF vehicle model (nonlinear model) and the actual vehicle test data during a constant-speed test. The test was conducted on a uniform, dry, level, and hard road surface.

A steering wheel angle of 125 degrees was used as step input, which was exerted for one second. Vehicle initial speed was at 30 km/h.

The vehicle model responses were well-matched with the actual vehicle measurements.

4. SBW modeling

The SBW system has three subsystems:

1. Steering wheel subsystem.
2. Front wheel subsystem.
3. ECU.

The steering wheel subsystem contains the torque sensor, steering angle sensor, and steering wheel motor. The steering wheel motor provides torque feedback to the driver, which allows the driver to feel the steering wheel position and vehicle motion.

The front wheel subsystem contains the position sensor,

[1] SAMAND vehicle (IRANKHODRO.CO) – Sedan Class Car, Ref. [8]

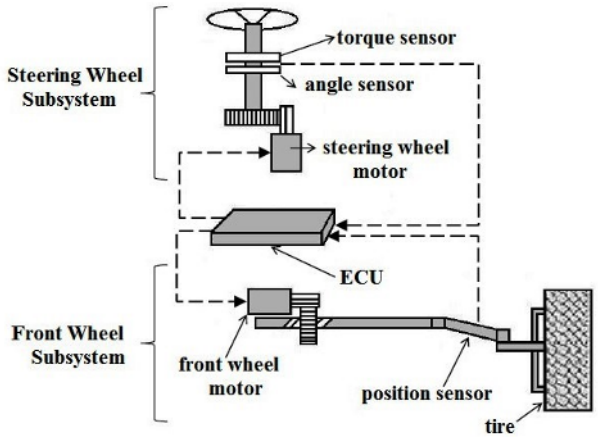

Fig. 7. SBW set-up.

rack pinion gear, front wheel motor, and other mechanical mechanisms. The front wheel motor positions the tire according to inputting data from the driver, which was obtained through the steering wheel subsystem.

The ECU controls the steering wheel motor and front wheel motor for the steering feel of the driver and for improving vehicle maneuverability and stability [1, 10]. Fig. 7 shows the three main parts of the SBW system.

A bond graph method is used to model the steering wheel subsystem and front wheel subsystem. A bond graph is a tool used to model complex multi-energy engineering systems (e.g., mechanical, electrical, and hydraulic subsystems).

A bond graph offers a suitable balance between specificity and generality for modeling complex physical systems. The interdisciplinary concept of energy and power flow creates a semantic level for bond graphs independent of the modeling domain. Therefore, the main advantage of this method is arguably the ability to model systems with elements from different energy domains. The bond graph method consists of the following element types:

Non-power source elements C, I , and R, which are passive one-port elements that include compliances, inductances, and resistances, respectively.

Power source elements S_e and S_f, which are active one-port elements that represent effort sources or flow sources, respectively.

Transformer (*TF*) and gyrator (*GY*), which are two-port elements; power is conserved in these elements.

Functions *0* and *1*, which are multi-port elements that represent series and parallel relations among elements (common effort or common flow) so that these elements are interconnected into the subsystem or system models [11].

4.1 Steering wheel subsystem modeling

The ECU produces input signals to control the reactive torque of the steering wheel motor by considering data from the sensors monitoring the steering wheel angle and steering column torque. The steering wheel, steering wheel motor, gear mechanism, and steering wheel column are modeled using the bond graph method. Table 1 shows the elements considered.

Table 1. Steering wheel subsystem elements.

Variable	Symbols used in the bond graph model
v_s	Se_2
R_{sa}	R_3
L_{sa}	I_3
J_{sm}	I_2
B_{sm}	R_2
C_{sm}	C_2
J_{sw}	I_1
B_{sw}	R_1
C_{sw}	C_1
T_d	Se_1
$1/G$	Transformer (TF) rate
K_{sb}	Gyrator (GY) rate

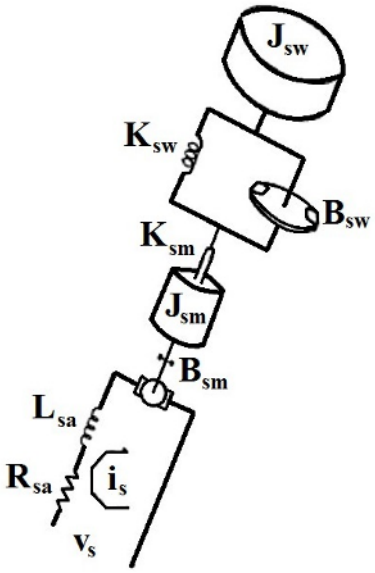

Fig. 8. Steering wheel subsystem mechatronics diagram.

Fig. 8 presents a mechatronics diagram of the steering wheel subsystem. Fig. 9 shows a bond graph model of the steering wheel subsystem. The state equations of the steering wheel subsystem are established using the bond graph method in Fig. 9.

Therefore, the equations are written as follows:

Equation for driver torque acting on the steering wheel

$$\dot{p}_2 = -\frac{B_{sw}}{J_{sw}} p_2 - \frac{1}{C_{sw}} q_5 + T_d \ . \tag{25}$$

Equation for angular velocity at the steering column

$$\dot{q}_5 = \frac{-GC_{sw}}{J_{sm}\left(C_{sw} + C_{sm}G^2\right)} p_{10} + \frac{C_{sw}}{J_{sw}\left(C_{sw} + C_{sm}G^2\right)} p_2 \ . \tag{26}$$

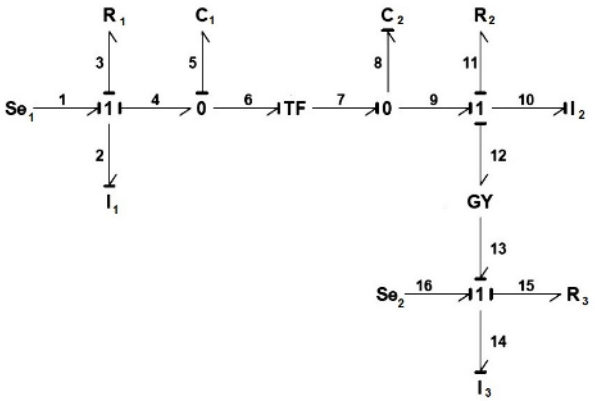

Fig. 9. Steering wheel subsystem bond graph model[2].

Equation for the torque at the steering wheel motor shaft before considering the compliance of the shaft (C_{sm})

$$\dot{p}_{10} = -\frac{K_{sb}}{L_{sa}} p_{14} - \frac{B_{sm}}{J_{sm}} p_{10} + \frac{G}{C_{sw}} q_5 \,. \tag{27}$$

Equation for steering wheel motor voltage at the inductance

$$\dot{p}_{14} = v_s - \frac{R_{sa}}{L_{sa}} p_{14} + \frac{K_{sb}}{J_{sm}} p_{10} \,. \tag{28}$$

Equation for the steering column angle

$$\delta_s = \frac{1}{J_{sw}} p_2 \,. \tag{29}$$

Consequently, the state equations of the steering wheel subsystem are as follows:

$$\begin{aligned} \dot{X}_s(t) &= A_s X_s(t) + B_s u_s(t) \\ y_s(t) &= C_s X_s(t) + D_s u_s(t) \end{aligned} \tag{30}$$

where the state vector is expressed as

$$X_s = \begin{bmatrix} p_{14} & p_{10} & p_2 & q_5 \end{bmatrix}^T \,. \tag{31}$$

The maximum voltage, which is supplied to the steering wheel motor, and applied driver torque are the input of the steering wheel subsystem as follows:

$$u_s(t) = \begin{bmatrix} v_s & T_d \end{bmatrix}^T \tag{32}$$

[2]Port numbers in the bond graph diagram are the subscripts of (p) or (q) in bond graph equations.

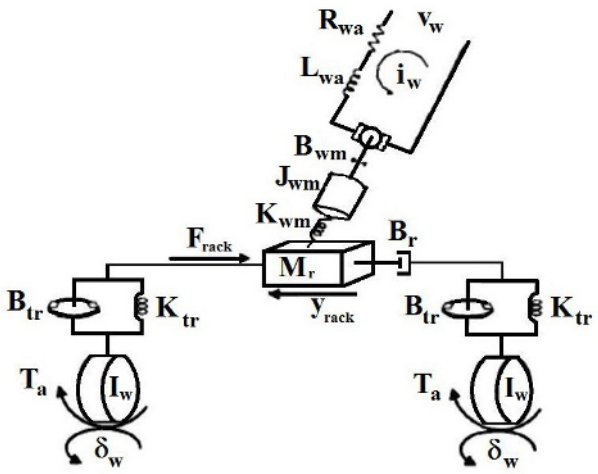

Fig. 10. Front wheel subsystem mechatronics diagram.

$$A_s = \begin{bmatrix} \frac{-R_{sa}}{L_{sa}} & \frac{K_{sb}}{J_{sm}} & 0 & 0 \\ \frac{-K_{sb}}{L_{sa}} & \frac{-B_{sm}}{J_{sm}} & 0 & \frac{G}{C_{sw}} \\ 0 & 0 & \frac{-B_{sw}}{J_{sw}} & \frac{-1}{C_{sw}} \\ 0 & \frac{-GC_{sw}}{J_{sm}\left(C_{sw}+C_{sm}G^2\right)} & \frac{C_{sw}}{J_{sw}\left(C_{sw}+C_{sm}G^2\right)} & 0 \end{bmatrix} \tag{33}$$

$$B_s = \begin{bmatrix} 1 & 0 & 0 & 0 \\ 0 & 0 & 1 & 0 \end{bmatrix}^T \tag{34}$$

$$C_s = \begin{bmatrix} 0 & 0 & \frac{1}{J_{sw}} & 0 \end{bmatrix}, \quad D_s = 0 \tag{35}$$

$$y_s(t) = \delta_s \,. \tag{36}$$

We have to note that

$$C_{sw} = \frac{1}{K_{sw}} \quad , \quad C_{sm} = \frac{1}{K_{sm}} \,. \tag{37}$$

4.2 Front wheel subsystem modeling

The front wheel subsystem includes the position sensor, rack pinion gear, front wheel motor, and other mechanical mechanisms. The ECU generates input signals to control the front wheel torque by obtaining the information from the position sensor monitoring rack bar displacement and integrating it with other information.

The front wheel motor, rack and pinion, tie rod, and tire are modeled using the bond graph method. Table 2 shows the elements considered.

Fig. 10 illustrates the mechatronics diagram of the front wheel subsystem. Fig. 11 depicts the bond graph model of the front wheel subsystem. The state equations of the front wheel subsystem are established using the bond graph method in Fig. 11.

Table 2. Front wheel subsystem elements.

Variable	Symbols used in bond graph model
v_w	Se_1
R_{wa}	R_1
L_{wa}	I_1
K_{wb}	Gyrator (GY) rate
J_{wm}	I_2
B_{wm}	R_2
C_{wm}	C_1
G_{mr}	Transformer 1 (TF_1) rate
M_r	I_3
B_r	R_3
C_{tr}	C_2
B_{tr}	R_4
I_w	I_4
T_a	Se_2
G_r	Transformer 2 (TF_2) rate

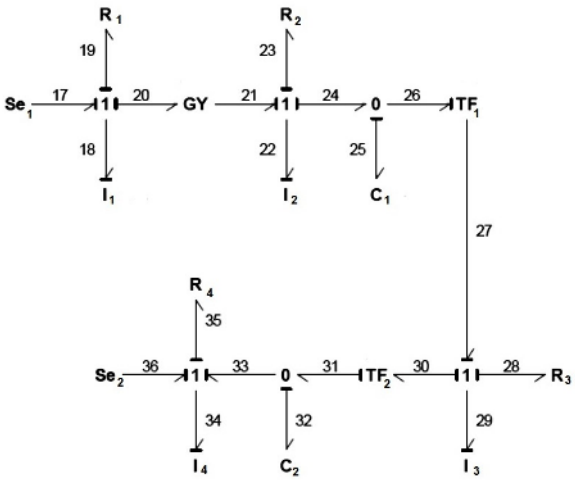

Fig. 11. Front wheel subsystem bond graph model.

The equations are written as follows:

Equation for front wheel motor voltage at inductance

$$\dot{p}_{18} = -\frac{R_{wa}}{L_{wa}} p_{18} - \frac{K_{wb}}{J_{wm}} p_{22} + v_w \,. \tag{38}$$

Equation for the torque at the front wheel motor shaft before considering the compliance of the shaft (C_{wm})

$$\dot{p}_{22} = \frac{K_{wb}}{L_{wa}} p_{18} - \frac{B_{wm}}{J_{wm}} p_{22} - \frac{1}{C_{wm}} q_{25} \,. \tag{39}$$

Equation for the angular velocity of the front wheel motor output shaft

$$\dot{q}_{25} = \frac{1}{J_{wm}} p_{22} - \frac{1}{G_{mr} M_r} p_{29} \,. \tag{40}$$

Equation for the force acting on the rack

$$\dot{p}_{29} = \frac{-B_r}{M_r} p_{29} + \frac{1}{G_{mr} C_{wm}} q_{25} - \frac{G_r}{C_{tr}} q_{32} \,. \tag{41}$$

Equation for the tie rod linear velocity

$$\dot{q}_{32} = \frac{1}{G_r M_r} p_{29} - \frac{1}{I_w} p_{34} \,. \tag{42}$$

Equation for the torque acting on the tire

$$\dot{p}_{34} = -\frac{B_{tr}}{I_w} p_{34} + \frac{1}{C_{tr}} q_{32} + T_a \,. \tag{43}$$

Equation for the front wheel angle

$$\delta_w = \frac{1}{I_w} p_{34} \,. \tag{44}$$

Consequently, the state equations of the front wheel subsystem are expressed as

$$\begin{aligned} \dot{X}_w(t) &= A_w X_w(t) + B_w u_w(t) \\ y_w(t) &= C_w X_w(t) + D_w u_w(t) \end{aligned} \tag{45}$$

where the state vector is expressed as

$$X_w = \begin{bmatrix} p_{18} & p_{22} & p_{29} & p_{34} & q_{25} & q_{32} \end{bmatrix}^T . \tag{46}$$

The voltage, which is supplied to the front wheel motor, and the self-aligning torque are the input of the front wheel subsystem, which is expressed as

$$u_w(t) = \begin{bmatrix} v_w & T_a \end{bmatrix}^T \tag{47}$$

$$A_w = \begin{bmatrix} \frac{-R_{wa}}{L_{wa}} & \frac{-K_{wb}}{J_{wm}} & 0 & 0 & 0 & 0 \\ \frac{K_{wb}}{L_{wa}} & \frac{-B_{wm}}{J_{wm}} & 0 & 0 & \frac{-1}{C_{wm}} & 0 \\ 0 & 0 & \frac{-B_r}{M_r} & 0 & \frac{1}{G_{mr} C_{wm}} & \frac{-G_r}{C_{tr}} \\ 0 & 0 & 0 & \frac{-B_{tr}}{I_w} & 0 & \frac{1}{C_{tr}} \\ 0 & \frac{1}{J_{wm}} & \frac{-1}{G_{mr} M_r} & 0 & 0 & 0 \\ 0 & 0 & \frac{1}{G_r M_r} & \frac{-1}{I_w} & 0 & 0 \end{bmatrix} \tag{48}$$

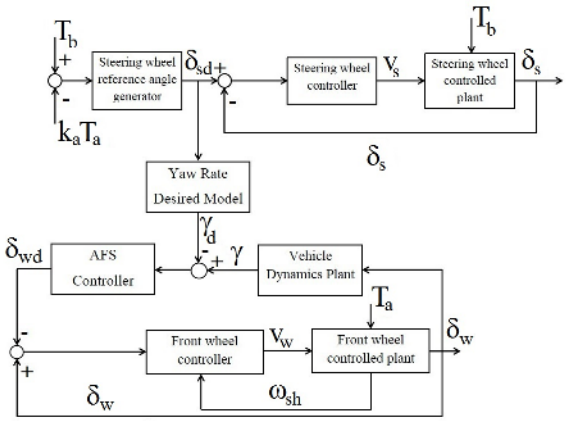

Fig. 12. SBW control block diagram.

$$B_w = \begin{bmatrix} 1 & 0 & 0 & 0 & 0 & 0 \\ 0 & 0 & 0 & 1 & 0 & 0 \end{bmatrix}^T \tag{49}$$

$$C_w = \begin{bmatrix} 0 & 0 & 0 & \dfrac{1}{I_w} & 0 & 0 \end{bmatrix}, \quad D_w = 0 \tag{50}$$

$$y_w(t) = \delta_w . \tag{51}$$

We have to note that

$$C_{tr} = \frac{1}{K_{tr}}, \quad C_{wm} = \frac{1}{K_{wm}} . \tag{52}$$

5. Control system design

Fig. 12 presents a block diagram of the SBW system control structure. The diagram includes the steering wheel motor controller, front wheel motor controller, and AFS controller.

The self-aligning torque is fed back to the steering wheel subsystem to inform the driver of road conditions.

Based on the control structure of the SBW system in Fig. 12, the steering wheel control subsystem produces a proper driver-adjustable steering feel whenever the driver holds or turns the steering wheel. Based on the variable steering ratio, a road wheel reference angle from the steering wheel angle is simultaneously given to the road wheel feedback control subsystem. The road wheel angle automatically tracks the steering wheel angle with minimal tracking error. When the driver releases the steering wheel, the road wheel angle and torque are provided as reference input signals to the steering wheel control subsystem to change the return rate and determine the steering wheel position. The steering wheel returns to the center or the desired angle with adjustable return rates in this case.

5.1 Active front steering controller

The AFS controller (yaw moment controller) is designed based on the SMC method to improve vehicle stability by tracking the reference yaw rate.

A driver intends to control the yaw rate when a vehicle travels around a corner. Consequently, the reference model reflects the desired relationship between the driver steer input and vehicle yaw rate. The reference model generates the yaw rate, which is chosen as the reference signal to be tracked through the active front steering controller. Therefore, the AFS controller forces the vehicle to follow the reference yaw rate through driving, which leads to a zero tracking error between the actual and desired yaw rates.

The AFS controller assists the driver in vehicle steering and in avoiding extreme handling situations, thereby contributing to vehicle stability and steerability. The AFS controller functions as a steering correction system by applying an additional steer angle to the one demanded by the driver.

$$\delta = \delta_c + \delta_w . \tag{53}$$

The 2-DOF model is the reference model for designing the AFS controller. Based on Eq. (24), the following equation is obtained:

$$\dot{\gamma} = a_{21} V_y + a_{22} \gamma + \frac{l_f C_f}{I_{zz}} \delta \tag{54}$$

where

$$\begin{aligned} a_{21} &= -\frac{\left(l_f C_f - l_r C_r\right)}{I_{zz} V_x} \\ a_{22} &= -\frac{\left(l_f^2 C_f + l_r^2 C_r\right)}{I_{zz} V_x} . \end{aligned} \tag{55}$$

The control in the SMC method forces system evolution on a certain surface, which guarantees the achievement of the control requirements [12]. To achieve the control objective (i.e., $\lim_{t\to\infty} S(t) = 0$), we define the sliding surface *S(t)* as

$$S = \gamma - \gamma_d . \tag{56}$$

The sliding condition *S(t)* = 0 implies a zero tracking error. Tracking time derivative of *S* gives

$$\dot{S} = \dot{\gamma} - \dot{\gamma}_d . \tag{57}$$

The trajectory of the closed-loop system is driven on Eq. (56) and evolves alongside it, achieving yaw stabilization by designing a satisfactory dynamics feedback control law. To obtain the control requirements, a reaching condition [13] is designed as

$$\dot{S} = -\lambda_1 S - \beta_1 \operatorname{sgn}\left(S\right) \tag{58}$$

where $\lambda_1 > 0$ is a control parameter that determines the convergence rate of a tracking error, $\beta_1 > 0$ is a control parameter that should be tuned according to the bound of uncertain-

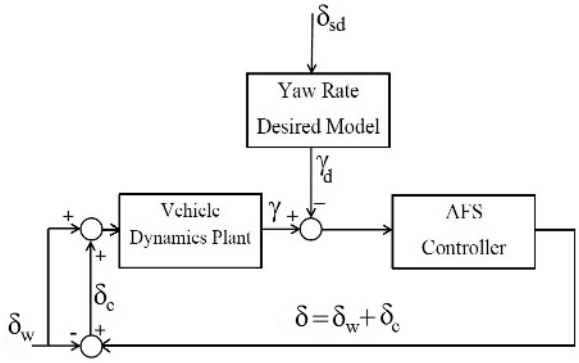

Fig. 13. AFS controller block diagram.

ties and disturbances, and sgn*(S)* is a sign function of *S*.

Substituting Eq. (54) into Eq. (57) yields

$$\dot{S} = a_{21}V_y + a_{22}\gamma + \frac{l_f C_f}{I_{zz}}\delta - \dot{\gamma}_d \,. \tag{59}$$

Thus, the best approximation $\hat{\delta}$ of a continuous control law that achieves $\dot{S} = 0$ is

$$\hat{\delta} = -\frac{I_{zz}}{l_f C_f}\left(a_{21}V_y + a_{22}\gamma - \dot{\gamma}_d\right). \tag{60}$$

Therefore, from Eqs. (58)-(60), the following equation is obtained:

$$\delta = -\frac{I_{zz}}{l_f C_f}\left(a_{21}V_y + a_{22}\gamma - \dot{\gamma}_d + \lambda_1(\gamma - \gamma_d) + \beta_1 \operatorname{sgn}(\gamma - \gamma_d)\right). \tag{61}$$

However, the presence of the discontinuous term, sign function (sgn) in Eq. (61) causes chattering, which involves extremely high control effort and excites high-frequency unmodeled dynamics [12]. The sign function is replaced with the saturation function, which is used to approximate a continuous control within a boundary layer around the sliding surface, to eliminate this effect. The saturation function is defined as

$$sat\left(\frac{S}{\varphi}\right) = \begin{cases} 1, & S/\varphi > 1 \\ S/\varphi, & -1 \le S/\varphi \le 1 \\ -1, & S/\varphi < -1 \end{cases} \tag{62}$$

where φ is the boundary layer thickness.

A desired yaw rate is dynamically calculated based on driver steering input and vehicle speed (Wong, 1993):

$$\gamma_d = \frac{V_x \delta_f}{l + K_u V_x^2} \tag{63}$$

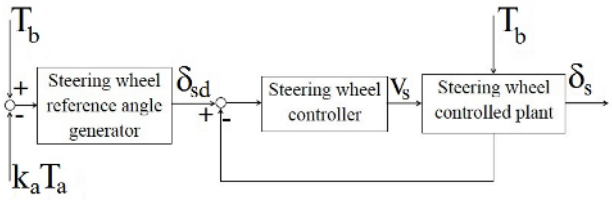

Fig. 14. Steering wheel motor controller block diagram.

where

$$K_u = m\left(\frac{l_r C_r - l_f C_f}{l C_f C_r}\right)$$
$$\delta_f = \frac{\delta_{sd}}{OSR}\,. \tag{64}$$

K_u is an under-steer parameter, l_rC_r-l_fC_f is a stability margin, *OSR* is the overall steering ratio (i.e., 17.4 in traditional vehicles), and δ_{sd} is the steering wheel reference angle.

5.1.1 AFS controller stability

The sliding mode control law Eq. (61) is proven to make the closed-loop control system asymptotically stable by introducing the positive definite Lyapunov function

$$V = \frac{1}{2}S^2 \,. \tag{65}$$

The time derivative of Eq. (65) is

$$\begin{aligned} \dot{V} &= S\dot{S} = S(\dot{\gamma} - \dot{\gamma}_d) \\ &= S\left(a_{21}V_y + a_{22}\gamma + \frac{l_f C_f}{I_{zz}}\delta - \dot{\gamma}_d\right) \\ &= S\left(-\lambda_1 S - \beta_1 \operatorname{sgn}(S)\right) \\ &= -\lambda_1 S^2 - \beta_1 |S| < 0 \,. \end{aligned} \tag{66}$$

Therefore, the control law Eq. (61) achieves the control objective (i.e., $S(t) \to 0$ as $t \to \infty$).

5.2 Steering wheel motor controller

The purpose of controlling the steering wheel motor is to improve driver steering feel through a reactive torque. The steering wheel motor controller is designed based on the PID control method because no consequential uncertainties exist in this system. The PID controller can also be a good controller.

Controller input is the steering wheel angle and controller output is the steering wheel motor voltage. The matrices A_s, B_s, C_s, and D_s obtained in the steering wheel subsystem modeling (see Section 4.1) with nominal values of steering parameters are used to derive the following transfer functions:

Table 3. Coefficients of transfer functions.

Coefficient	Magnitude
n_1	2.5∗10
n_2	$1.5837*10^4$
n_3	$2.5259*10^6$
n_4	$1.2671*10^9$
m_1	$1.1369*10^{-13}$
m_2	$5.8208*10^{-11}$
m_3	$-1.4901*10^{-8}$
m_4	$-6.9063*10^8$
d_1	$6.391*10^2$
d_2	$1.0864*10^5$
d_3	$5.3816*10^7$
d_4	$3.6648*10^8$

$$\frac{\delta_s}{v_s} = \frac{n_1 S^3 + n_2 S^2 + n_3 S + n_4}{S^4 + d_1 S^3 + d_2 S^2 + d_3 S + d_4} \tag{67}$$

$$\frac{\delta_s}{T_d} = \frac{m_1 S^3 + m_2 S^2 + m_3 S + m_4}{S^4 + d_1 S^3 + d_2 S^2 + d_3 S + d_4} \tag{68}$$

where n_i, m_i, and d_i are mentioned in Table 3.

The mechanical model (conventional model) of the steering wheel system is the reference model of this controller. Therefore,

$$J_s \ddot{\delta}_{sd} + B_s \dot{\delta}_{sd} + K_s \delta_{sd} = T_b - k_a T_a \tag{69}$$

where T_b is a torsion bar torque

$$T_b = K_{bd} T_d \tag{70}$$

where T_d is a driver torque, K_{bd} is the ratio between the torsion bar torque and driver torque, k_a is a scale factor, and T_a is a self-aligning torque in the linear tire model defined as

$$T_a = \left(t_p + t_m\right) F_{yf} \tag{71}$$

where t_p and t_m are the tire pneumatic and mechanical trails, respectively. J_s, B_s, and K_s are the total moment of inertia, resistance, and stiffness coefficients of the steering wheel system, respectively.

5.3 Front wheel motor controller

The purpose of controlling the front wheel motor is to improve maneuverability and stability through front wheel steering. Controller input is the front wheel angle and controller output is the front wheel motor voltage. This controller is designed based on the SMC method using the following equations:

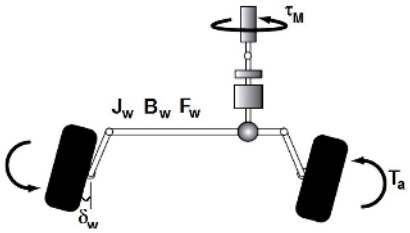

Fig. 15. Front wheel subsystem dynamics.

$$J_w \ddot{\delta}_w + B_w \dot{\delta}_w + T_f = r_s \tau_M - T_a \,. \tag{72}$$

Motor equations are as follows:

$$\tau_M = K_{wb} \kappa i_w \,, \quad E = K_{wb} \omega_{sh} \tag{73}$$

$$v_w = E + R_{wa} i_w \,. \tag{74}$$

Combining Eqs. (72)-(74), we obtain the following equation:

$$\begin{aligned} \ddot{\delta}_w &= \frac{r_s \kappa K_{wb}}{R_{wa} J_w} v_w + f \\ f &= -\frac{B_w}{J_w} \dot{\delta}_w - \frac{r_s \kappa K_{wb}^2}{R_{wa} J_w} \omega_{sh} - \frac{1}{J_w}\left(T_f - T_a\right) \end{aligned} \tag{75}$$

where J_w and B_w are the total moments of inertia of the front wheel system, r_s is the steering ratio, κ is the motor efficiency, ω_{sh} is the angular velocity of the motor output shaft, and T_f is the friction torque defined as

$$T_f = 9.8 \mu F_w t_p \operatorname{sgn}\left(\dot{\delta}_w\right) \tag{76}$$

where F_w is the front wheel weight and μ is the friction coefficient.

The dynamic f is not exactly known but estimated as $\hat{f}$. The estimation error is assumed to be bounded by some known function $F = F\left(\delta_w, \dot{\delta}_w\right)$ as follows:

$$\left| f - \hat{f} \right| \le F \,. \tag{77}$$

The control objective drives the state δ_w to the reference value δ_{wd}. A switching surface S is defined as

$$S = \dot{\tilde{\delta}}_w + \lambda_2 \tilde{\delta}_w \tag{78}$$

where λ_2 is a positive parameter. The tracking error in variable δ_ω is

$$\tilde{\delta}_w = \delta_w - \delta_{wd} \,. \tag{79}$$

Then,

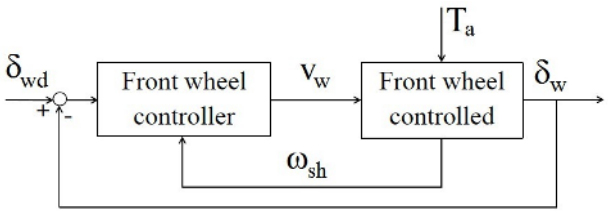

Fig. 16. Front wheel motor controller block diagram.

$$\dot{S} = \dddot{\tilde{\delta}}_w + \lambda_2 \ddot{\tilde{\delta}}_w$$
$$\dot{S} = \frac{r_s \kappa K_{wb}}{R_{wa} J_w} v_w + f + \lambda_2 \left(\ddot{\delta}_w - \ddot{\delta}_{wd} \right) - \dddot{\delta}_{wd} \,. \tag{80}$$

Thus, the best approximation $\hat{v}_w$ of a continuous control law that achieves $\dot{S} = 0$ is

$$\hat{v}_w = -\frac{R_{wa} J_w}{r_s \kappa K_{wb}} \left(\hat{f} + \lambda_2 \left(\ddot{\delta}_w - \ddot{\delta}_{wd} \right) - \dddot{\delta}_{wd} \right). \tag{81}$$

To satisfy the sliding condition despite uncertainty on dynamics f, we add a discontinuous term to $\hat{v}_w$ as follows:

$$v_w = \hat{v}_w - \beta_2 \operatorname{sgn}(S). \tag{82}$$

From Eqs. (80)-(82), the following equation is obtained:

$$\dot{S} = f - \hat{f} - \frac{r_s \kappa K_{wb}}{R_{wa} J_w} \beta_2 \operatorname{sgn}(S). \tag{83}$$

β_2 is chosen as

$$\beta_2 = \frac{R_{wa} J_w}{r_s \kappa K_{wb}} (F + \eta) \tag{84}$$

where η is a strictly positive constant.

The discontinuous switching, sign function sgn (S) results in chattering during the sliding motion. The sign function is replaced with the saturation function to eliminate this effect.

$$v_w = \hat{v}_w - \beta_2 sat(\frac{S}{\varphi}) \tag{85}$$

The AFS controller is an upper-level controller for the front wheel motor controller. Therefore, the following equation is considered in the SBW control block diagram:

$$\delta_{wd} = \delta \tag{86}$$

where δ is the AFS controller output.

5.3.1 Front wheel motor controller stability

The Lyapunov candidate function is selected as

Table 4. Laden and unladen vehicle parameters.

Parameter	Unladen	Laden
m	1300 kg	1600 kg
I_{zz}	1808.8 kg.m^2	1991 kg.m^2
l_f	1.2247 m	1.315 m
l_r	1.4373 m	1.347 m

$$V = \frac{1}{2} S^2 \,. \tag{87}$$

System stability is immediately verified and the sliding condition is satisfied as follows:

$$\dot{V} = \frac{1}{2} \frac{d}{dt} S^2 = S\dot{S} = S\left(f - \hat{f} - \frac{r_s \kappa K_{wb}}{R_{wa} J_w} \beta_2 \operatorname{sgn}(S) \right). \tag{88}$$

The following equation is obtained from Eq. (84):

$$\begin{aligned} \dot{V} &= \frac{1}{2} \frac{d}{dt} S^2 = S\dot{S} = S\left(f - \hat{f} - (F + \eta) \operatorname{sgn}(S) \right) \\ &= (f - \hat{f}) S - (F + \eta) |S| \\ &= (f - \hat{f}) S - \left| (f - \hat{f}) S \right| - \eta |S| \le -\eta |S| \,. \end{aligned} \tag{89}$$

Therefore, the sliding condition is satisfied [12].

6. Results

During vehicle design, development, and improvement, the vehicle is first evaluated using computer simulation software. The designed system or subsystem is then evaluated on a real vehicle and proving ground.

The SBW vehicle and conventional vehicle are evaluated in the single-lane-change maneuver on a dry road to evaluate the control structure performance obtained in this study. The vehicle moves at an initial speed of 100 km/h and has a friction coefficient of 0.9. The vehicle is in laden condition. The unladen and laden parameters of the vehicle are shown in Table 4.

The driver exerts a torque on the steering wheel to access to the single-lane-change maneuver (Fig. 17). The steering wheel needs to rotate within the desirable angle δ_{sd} in reference to Eqs. (70) and (71). The motor behind the steering wheel produces a voltage to create resistance for the steering feel of the driver. Fig. 18 explains how the actual steering angle follows the target angle precisely. The PID controller leads the ultimate steering wheel angle toward the target angle.

Fig. 19 illustrates the vehicle yaw rate. First, the similarity between the yaw rate amount in the laden and unladen vehicles indicates the robustness of the AFS controller, which is designed to control the vehicle yaw rate. Second, the SBW

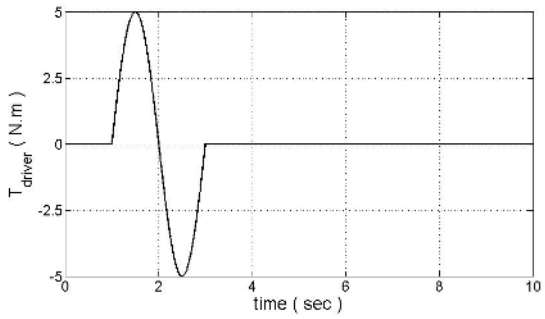

Fig. 17. Driver torque.

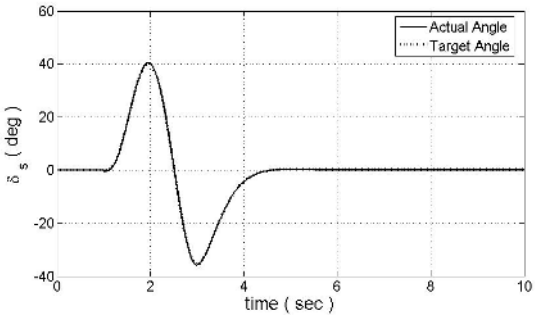

Fig. 18. Steering wheel angle.

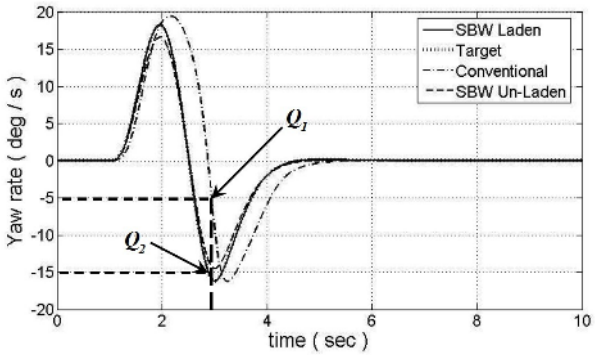

Fig. 19. Vehicle yaw rate.

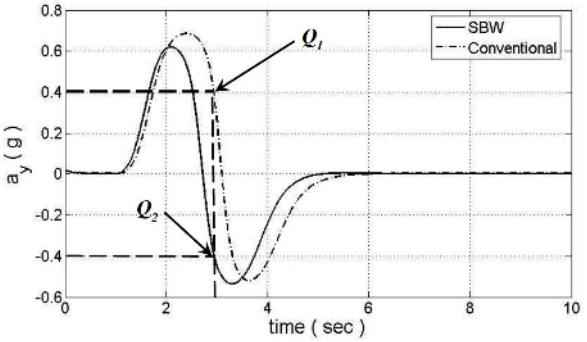

Fig. 20. Lateral acceleration of vehicle body.

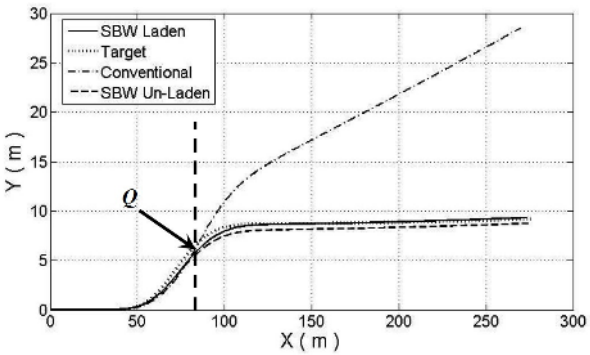

Fig. 21. Vehicle path.

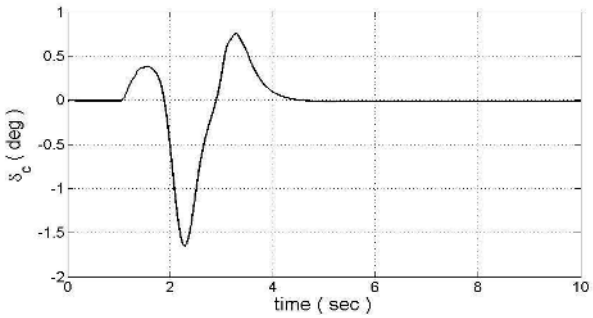

Fig. 22. Corrective angle of AFS controller.

vehicle yaw rate at the third second of motion is almost -15 deg/s (Q_2), which is close to the target. The conventional vehicle yaw rate is -5 deg/s (Q_1).

This target value difference significantly influences the lateral acceleration of the conventional vehicle (Fig. 20). The lateral acceleration for the conventional vehicle at a moment of motion is 0.4 g, and the value for the SBW vehicle is -0.4 g. Consequently, the conventional vehicle lateral force, which is a lateral acceleration function, is in the opposite direction of the SBW vehicle lateral force.

The difference between lateral forces causes the conventional vehicle to lose stability and go off-target (Fig. 21). The vehicle covers 85 meters of the path in x direction at the third second of motion. The conventional vehicle at moment (Q) deviates from the desired vehicle path (Fig. 21). This deviation increases dramatically. Thus, the conventional vehicle can never return to the desired path and becomes unstable. Moreover, the distances covered by the laden and unladen vehicles are almost the same. The distance covered by the conventional vehicle is different from the desired distance.

The AFS controller corrects the front wheel angle. The angle added to correct the front wheel angle is shown in Fig. 22. The front wheel angle is illustrated in Fig. 23.

The front wheel motor and steering wheel motor maximum torques are shown in Figs 24 and 25, respectively. The steering wheel motor is a brushed DC motor that has a rated torque of 0.5 Nm for 1026 rpm. The front wheel motor is a brushless AC motor that has a maximum torque of 15 Nm for 500 rpm.

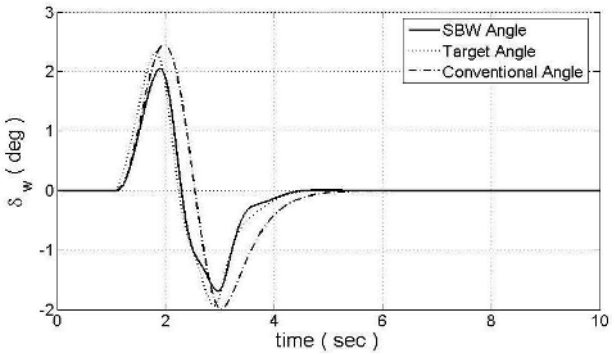

Fig. 23. Front wheel angle.

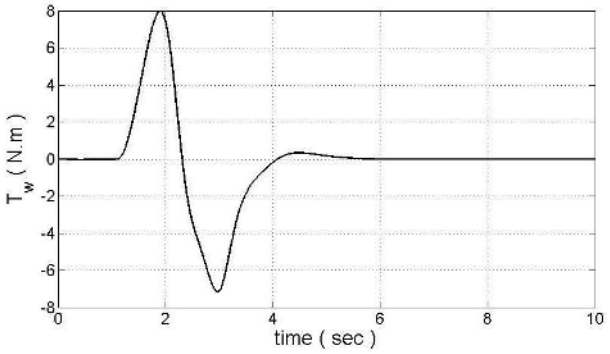

Fig. 24. Front wheel motor maximum torque.

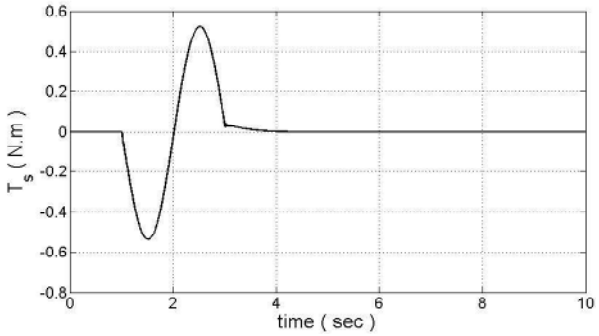

Fig. 25. Steering wheel motor maximum torque.

7. Steering feel

The steering feel provides information on contact surfaces between vehicle tires and the ground. Therefore, the steering feel is significant to the driver for vehicle direction control and driving safety. In a conventional steering system with mechanical connections, a driver directly controls the vehicle direction by turning the steering wheel, which obtains a steering feel through the mechanical steering mechanism. The tire force should be fed back to the steering wheel in the SBW system without mechanical connection between the steering wheel and road wheels. The self-aligning torque is fed back to the steering wheel to inform the driver of road conditions.

The sinusoidal maneuver is used to evaluate driver steering feel in this study.

The torque reaction of the steering wheel determines the steering feel. When holding the steering wheel, the driver directly produces a torque reaction through the steering wheel shaft in the conventional steering system. The steering wheel motor provides the steering wheel torque in the SBW system.

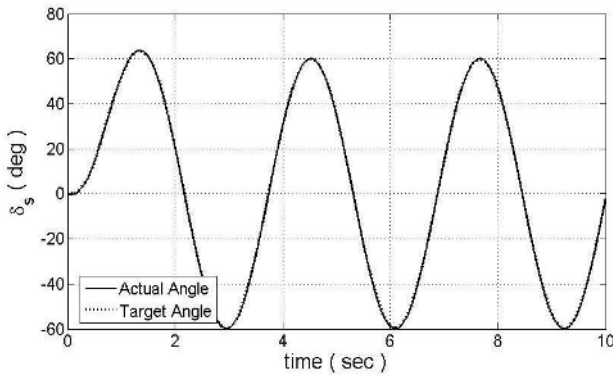

Fig. 26. Steering wheel angle.

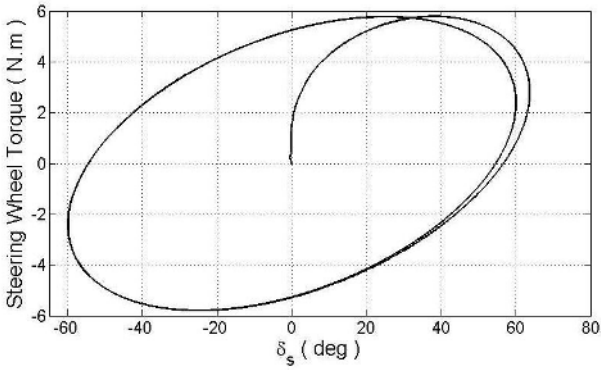

Fig. 27. Steering feel of driver.

8. Conclusion and future research

A nonlinear 8-DOF vehicle model incorporating the magic formula tire model was used to simulate a vehicle in this study. The AFS and front wheel motor controllers are designed based on the SMC method. These controllers improve vehicle stability and maneuverability. The steering wheel motor controller is designed based on the PID control method. This controller effectively controls the motor, thereby providing the steering feel to the driver. The proposed control system guarantees high robustness for changing conditions of vehicle weight and various severe driving conditions (i.e., lane-change and sinusoidal maneuvers).

This study can be further improved by integrating the brake-by-wire (BBW) system and other brake systems with the SBW vehicle and evaluating vehicle performance. Other

methods for controller design can be used to compare various types of control methods. Moreover, designing estimators and observers to estimate the mass, moments of inertia of the vehicle, and longitudinal and lateral forces of the tire is beneficial in evaluating the effects of these elements on the actual performance of the vehicle.

Nomenclature

C_f, C_r : Front and rear cornering stiffness of tire
$C_{\phi f}$, $C_{\phi r}$: Front and rear roll damping coefficient
$K_{\phi f}$, $K_{\phi r}$: Front and rear roll stiffness
l_f, l_r : Distance from the CG to the front and rear axle
d : Wheel track width
h_s : Length of the roll moment arm
h : Height of center of gravity
I_w : Wheel moment of inertia about the spin axis
I_{xx} : Roll moment of inertia
I_{zz} : Yaw moment of inertia
I_{xz} : Product of inertia about roll and yaw axes
m, m_s : Total mass, sprung mass of the vehicle
R_w : Effective wheel rolling radius
ϕ : Roll angle
γ : Yaw angle
α : Tire side slip angle
V_x : Longitudinal vehicle velocity
V_y : Lateral vehicle velocity
a_x : Longitudinal acceleration of the vehicle body
a_y : Lateral acceleration of the vehicle body
δ_w : Front wheel angle
δ_s : Steering wheel angle
v_s : Voltage of the steering wheel motor
i_s : Current of the steering wheel motor
R_{sa} : Steering wheel motor resistance
L_{sa} : Steering wheel motor inductance
K_{sb} : Steering wheel motor torque constant
J_{sm} : Steering wheel motor moment of inertia
B_{sm} : Steering wheel motor resistance coefficient
C_{sm} : Compliance of the steering wheel motor shaft
J_{sw} : Steering wheel and column moment of inertia
B_{sw} : Resistance at the steering column
C_{sw} : Compliance of the steering column
G : Reduction ratio of gear mechanism
v_w : Voltage of the front wheel motor
i_w : Current of the front wheel motor
R_{wa} : Front wheel motor resistance
L_{wa} : Front wheel motor inductance
K_{wb} : Front wheel motor torque constant
J_{wm} : Front wheel motor moment of inertia
B_{wm} : Front wheel motor resistance coefficient
C_{wm} : Compliance of the front wheel motor shaft
G_{mr} : Radius of the pinion
M_r : Mass of the rack
B_r : Resistance of the rack
C_{tr} : Compliance of the tie rod
B_{tr} : Resistance of the tie rod
T_a : Self-aligning torque
G_r : Length ratio of the steering arm
g : Gravity of the Earth

References

[1] S. Jang, T. Park and C. S. Han, A control of vehicle using steer-by-wire system with hardware-in-the-loop-simulation system, *International Conference on Advanced Intelligent Mechatronics (AIM), IEEE/ASME* (2003).

[2] R. Hayama, K. Nishizaki and S. Nakano, The vehicle stability control responsibility improvement using steer-by-wire, *Proceedings of IEEE Intelligent Vehicles Symposium* (2000) 596-601.

[3] P. Setlur, D. Dawson, J. Wagner and Y. Fang, Nonlinear tracking controller design for steer-by-wire automotive systems, *Proceedings of the American Control Conference,* Anchorage, AK (2002) 280-285.

[4] T. Park, C. Han and S. Lee, Development of the electronic control unit for the rack-actuating steer-by-wire using the hardware-in-the-loop simulation system, *Mechatronics Journal,* Elsevier, 15 (2005) 889-918.

[5] N. Bajcinca and R. Cortesao, Robust control for steer-by-wire vehicles, *Autonomous Robots Journal,* Springer Science, 19 (2005) 193-214.

[6] J. Sung, F. Ozaki, T. Matsushita and S. Kawaji, Experimental study on steer-by-wire system with bilateral control, *Proceeding of International Conference on Mechatronics* (2007).

[7] H. B. Pacejka, *Tire and vehicle dynamics,* John Wiley & sons, 2nd Edition.

[8] Wong, *Theory of ground vehicle,* Jon Wiley & sons, 2nd edition (1993).

[9] Kevan Granat, Steady-state directional control test procedures for passenger cars and light trucks, *SAE J266* (2002).

[10] Y. Yao, Vehicle steer-by-wire system control, *SAE technical paper,* no. 2006-01-1157 (2006).

[11] C. Karnopp, *System dynamics-modeling and simulation of mechatronic systems,* 4th edition, Wiley & sons (2006) 34-76.

[12] Slotine. Li, *Applied nonlinear controller,* Prentice Hall (1991) 276-310.

[13] Dean Karnopp, *Vehicle Stability*, Marcel Dekker (2004).

[14] I. Mousavinejad and R. Kazemi, Robust controller design to develop the front wheel subsystem of steer-by-wire system, *Proceeding of CACS International Automatic Control Conference (IACC),* Nov 27-29 (2009).

[15] R. Kazemi and I. Mousavinejad, A comprehensive model for developing of steer-by-wire system, WASET, International Science Index 56, *International Journal of Mechanical, Industrial Science and Engineering*, 5 (8) (2011) 2-8.

[16] I. Mousavinejad, R. Kazemi and M. B. Khaknejad, Nonlinear controller design for active front steering system, WASET, International Science Index 61, *International*

Journal of Mechanical, Industrial Science and Engineering, 6 (1) (2012) 6-11.

[17] I. Mousavinejad, *Nonlinear controller design for steer-by-wire passenger car*, M.Sc. thesis, Sharif University of Technology (2009).

[18] R. Kazemi and A. A. Janbakhsh, Nonlinear adaptive sliding mode control for vehicle handling improvement via steer-by-wire, *International Journal of Automotive Technology* (2010).

[19] A. A. Janbakhsh and R. Kazemi, A new approach to enhance vehicle maneuverability performance using SBW system, *Proceeding of ISIE 2009, IEEE International Symposium on Industrial Electronics* (2009).

[20] A. A. Janbakhsh and R. Kazemi, A New approach for simultaneous vehicle handling and path tracking improvement through SBW system, *Proceeding of International Conference ASME* (2010).

[21] Seongi in Yim, Design of a robust controller for rollover prevention with active suspension and differential braking, Springer, *Journal of Mechanical Science and Technology,* 26 (1) (2012) 213-222.

[22] Ju Young Choi, Robust controller for an autonomous vehicle with look-ahead and look-down information, Springer, *Journal of Mechanical Science and Technology*, 25 (10) (2011) 2467-2474.

Appendix

Table 5. Vehicle parameter values.

Variable name	Variable magnitude	Variable unit
m	1300	Kg
m_s	1167	Kg
l_f	1.2247	m
l_r	1.4373	m
d	1.4376	m
h	0.5253	m
h_s	0.445	m
I_{xx}	346.7	Kg m^2
I_{zz}	1808.8	Kg m^2
I_{xz}	21.09	Kg m^2
I_w	2.11	Kg m^2
R_w	0.285	m
$K_{\phi f}$	66175	Nm/rad
$K_{\phi r}$	66175	Nm/rad
$C_{\phi f}$	3511	Nm s/rad
$C_{\phi r}$	3511	Nm s/rad
g	9.81	m/s^2
C_f	165000	N/rad
C_r	165000	N/rad

Table 6. Steering system parameter values.

Symbol	Variable magnitude	Variable unit
J_{sw}	0.04	Kg m^2
B_{sw}	0.225	Nm s/rad
C_{sw}	5.8*10^{-3}	rad/(Nm)
J_{sm}	4.8*10^{-4}	Kg m^2
B_{sm}	3.4*10^{-3}	N/(m/s)
C_{sm}	1.59*10^{-3}	Nm rad/s
R_{sa}	0.1685	ohm
L_{sa}	2.69*10^{-4}	henry
K_{sb}	0.045	Nm/A ; V/(rad/s)
G	0.49	-
G_{mr}	7.367*10^{-3}	m
G_r	1	-
M_r	2	Kg
B_r	90	Nm s/rad
R_{wa}	0.21	ohm
L_{wa}	0.52*10^{-3}	henry
K_{wb}	0.65	Nm/A; V/(rad/s)
J_{wm}	9.8*10^{-4}	Kg m^2
B_{wm}	5.7*10^{-4}	N/(m/s)
C_{wm}	1.29*10^{-3}	Nm rad/s
C_{tr}	6.72*10^{-5}	rad/Nm
B_{tr}	40	Nm s/rad

Iman Mousavinejad received a B.S. degree in Mechanical Engineering from Islamic Azad University, and an M.S. degree in Mechatronics Engineering from Sharif University of Technology, Iran, in 2009. His research interests include vehicle dynamics and control, autonomous vehicles, mechatronics, drive assistance systems, by-wire technology, and vehicle control.

Reza Kazemi received B.S. and M.S. degrees in Mechanical Engineering from Isfahan University of Technology, and a Ph.D. in Mechanical Engineering from Amir Kabir University of Technology, Iran, in 2000. He is currently an associate professor at the Mechanical Engineering department, Khaje Nasir Toosi University of Technology, Tehran, Iran. His research interests include vehicle dynamics and control, drive assistance systems, optimal control, fuzzy control, by-wire technology, and vehicle control. Dr. Kazemi received the Best Professor and National Superior Ideas awards in 2012.